Nuclear Instruments and Methods in Physics Research B 502 (2021) 66–72

Contents lists available at ScienceDirect

Nuclear Inst. and Methods in Physics Research, B

journal homepage: www.elsevier.com/locate/nimb

Effect of thermal annealing on SHI irradiated indium implanted glassy carbon

E.G. Njoroge [a,b,*], T.T. Hlatshwayo [a], M. Mlambo [a], O. Odutemowo [a], K.A. Annan [c], V. A. Skuratov [d,e,f], M. Ismail [g], J.B. Malherbe [a]

[a] Department of Physics, University of Pretoria, Pretoria, South Africa
[b] ENGAGE, University of Pretoria, Pretoria, South Africa
[c] Department of Materials Science and Metallurgical Engineering, University of Pretoria, Pretoria, South Africa
[d] Joint Institute for Nuclear Research, Dubna, Russia
[e] National Research Nuclear University MEPhI, Moscow, Russia
[f] Dubna State University, Dubna, Russia
[g] Department of Physics, University of Zalingei, Zalingei, Central Darfur, Sudan

ARTICLE INFO

Keywords:
Ion implantation
SHI irradiation
Diffusion
Glassy carbon
Indium
RBS

ABSTRACT

The effects of swift heavy ion irradiation on implanted glassy carbon, the modification and migration of indium after vacuum annealing have been investigated. Radiation damage was introduced to the glassy carbon substrates after room temperature implantation by 360 keV indium ions to a fluence of 2.0×10^{16} ions/cm ^{2}. The implanted samples were subsequently irradiated at room temperature by swift heavy ions (167 MeV Xe $^{26+}$ ions). Isochronal annealing of both sets of samples from 200 to 600 °C for 1 h was performed in vacuum. The SHI irradiation, induced some restructuring in the damaged glassy carbon substrates. Vacuum annealing of the SHI irradiated samples gave rise to recovery and the diffusion of implanted In which was different from that of the as-implanted sample. Higher retention was observed at each temperature for SHI irradiated samples compared to as-implanted samples. The diffusion coefficients of the SHI irradiated samples were lower than for un-irradiated sample.

1. Introduction

Glassy carbon or vitreous carbon is synthetically prepared by slow and controlled pyrolysis of organic resin precursors at temperatures higher than 900 °C under an inert atmosphere [1]. Glassy carbon is considered to be a disordered carbon material that is non-graphitizing and is stable at high temperatures of up to 3000 °C [2]. It has a turbostratic structure that consists of graphite-like ribbons or microfibrils (with in-plane cluster size, $L_a < 40$ Å), in which the carbon atoms are primarily sp^2 hybridized [3]. The glassy carbon structure has been reported to be related to that of fullerenes, where pentagons and heptagons are distributed among hexagons to form curved graphite planes [4,5]. This leads to a glassy carbon structure consisting of a complicated network that has some microstructural disorder, and long-range order does not exist [6]. Therefore, glassy carbon has graphitic ordering between that of highly oriented pyrolytic graphite (HOPG) and amorphous carbon.

This material has very attractive properties (summarised in ref [7]) that are a combination of ceramic and graphitic properties, which make glassy carbon have the potential for future technological and industrial applications [8]. Glassy carbon, which does not graphitize at temperatures < 3000 °C, has a lower density of 1.42 g/cm^3 compared to 2.3 g/cm^3 for graphite and 3.52 g/cm^3 for diamond [9]. Despite the low density, glassy carbon has high hardness, which exceeds that of graphite [10].

Glassy carbon is a technologically important material for the nuclear industry and related applications. It has been proposed as a containment material of radioactive waste from nuclear reactors [11]. This material can act as a protective layer on the surface of graphite reactor cores and in molten salt reactors cooling pipes [12]. In such nuclear applications, glassy carbon would be exposed to a radiation harsh environment, therefore its resistance to radiation damage has been a subject of some previous studies [3,7,13–15]. Indium implantation into glassy carbon has been previously reported to induce damage or disorder in the near-surface regions of glassy carbon [7]. The damage by ion bombardment can lead to an increase in density within the implanted region [13–15].

* Corresponding author at: Department of Physics, University of Pretoria, Pretoria, South Africa.
E-mail address: eric.njoroge@up.ac.za (E.G. Njoroge).

https://doi.org/10.1016/j.nimb.2021.06.011
Received 12 November 2020; Received in revised form 13 June 2021; Accepted 16 June 2021
Available online 22 June 2021

Swift heavy ions (SHI) lose energy as they traverse a material through localized electronic excitations (electronic energy loss) along the ion trajectories, which induces a transient melting phase known as a thermal spike [13]. SHI irradiation can modify material structure and properties, introduce defects by the rapid quenching, or anneal pre-existing defects due to the localised high temperatures involved.

Investigations on ion implantation damage and swift heavy ion induced restructuring of glassy carbon are important since this material has promising nuclear applications. In such applications glassy carbon should be stable under irradiation with MeV energy heavy ions and maintain its structure. In this study, we focus on Rutherford backscattering spectrometry (RBS) and Raman spectroscopic investigations on the effects of annealing and SHI irradiation on indium implanted glassy carbon. The step height measurements between un-implanted and implanted regions by a profilometer were performed so that changes in the density of the modified region could be examined. The diffusion coefficients of indium in glassy carbon after annealing the as-implanted and the implanted then SHI irradiated samples will be calculated and compared. A literature survey indicated that the diffusion coefficients obtained after annealing implanted glassy carbon (summarised in [16]) but there is no diffusion coefficient data reported for ions implanted in glassy carbon after swift heavy ion irradiation.

2. Experimental method

The substrates used in this study were the commercially available Sigradur® G glassy carbon strips with a density of 1.42 g/cm^3. The strips were cut into 1 × 1 cm^2 samples by a rotary saw. Indium implantation into glassy carbon was performed at room temperature at the energy of 360 keV to a fluence of 2.0 × 10^{16} ions/cm^2 at the Friedrich-Schiller-Universität, Jena, Germany. Masks were used to obtain implanted and pristine areas on the glassy carbon substrate. Two indium implanted glassy carbon samples were irradiated at room temperature by 167 MeV Xe^{26+} to fluences of 3.4 × 10^{14} and 8.3 × 10^{14} ions/cm^2. The first set of samples, that is as-implanted, were annealed between 200 and 600 °C for 1 h. Then the second set of samples, that is, implanted and then SHI irradiated to different fluences, were also annealed from 200 to 600 °C for 1 h.

Raman spectroscopic analysis of glassy carbon after indium implantation, SHI irradiation, and sequential vacuum annealing was performed using argon laser operating at 514.5 nm wavelength. The indium depth profiles were monitored after annealing of as-implanted samples and the implanted then SHI irradiated samples by Rutherford backscattering spectrometry (RBS) using 1.6 MeV $^4He^+$ ions. A silicon surface barrier detector at a backscattering angle of 165° was used to detect the backscattered particles.

3. Results and discussion

3.1. Thermal annealing of RT implanted glassy carbon

We investigated the densification or compaction of glassy carbon after the indium implantation. Step height measurements between the implanted and un-implanted regions were performed using a profilometer. The density was calculated using the procedure elaborated in ref [17]. The indium implantation produced a compacted and denser damaged region with an average density of about 2.04 g/cm^3. This density is higher than that of pristine glassy carbon but lower than that of graphite.

Compaction of the glassy carbon structure following ion implantation can be understood when the porous nature of the glassy carbon structure is considered. During implantation, the glassy carbon structure was damaged and the turbostratic structure (graphitic ribbons) broke down. The number of nano-pores also decreased leading to increased impermeability.

The depth distribution of implanted indium, the theoretical distribution, the damage profile and the electronic energy loss due to SHI in glassy carbon were calculated using the SRIM code [18] with density of 2.04 g/cm^3. The SRIM simulations were performed using the "Full cascade" option and with threshold displacement energy of 25 eV for carbon. These profiles are shown in Fig. 1. The use of higher density for SRIM calculations has been used by other authors [3,19]. The projected range (R_p) and range straggling (ΔR_p) values of 154 nm and 30 nm, respectively were obtained by fitting the as-implanted indium profile. The damage profile had a maximum of 34 dpa at about 120 nm below the surface. Therefore, the near-surface region of the glassy carbon substrate was expected to be damaged by the indium implantation. The depth distribution of room temperature implanted 360 keV indium ions into glassy carbon to a fluence of 2 × 10^{16} cm^{-2} and the theoretical profile obtained by SRIM simulations can be observed to be nearly Gaussian. The experimental projected range is slightly lower than the theoretical and the experimental profile is also slightly broader.

The diffusion of indium after sequential annealing of the as-implanted and the implanted then SHI irradiated samples were investigated using RBS analysis. Fig. 2 shows the indium depth profiles pre and post sequential annealing of the as-implanted samples for 1 h from 200 °C to 600 °C. After annealing at 200 °C, the indium profile was similar to the as-implanted one and the implanted indium was stable.

Annealing at 300 °C, led to a slight broadening of the indium depth with migration of implanted indium towards the surface and towards the less damaged bulk. The amount of implanted indium retained within the glassy carbon is plotted in Fig. 3 and it can be observed that after annealing at 300 °C it is still the same as the as-implanted. At 400 °C, the indium profile broadened further with a small fraction of the implanted indium diffusing towards the bulk. Migration of indium towards the glassy carbon surface, which is the more damaged region was observed to be significant at this temperature. It can also be seen that the projected range did not shift at this temperature and the profile was approximately centered at the as-implanted R_p of 154 nm. This kind of symmetric broadening of the implanted indium profile is characteristic of Fickian diffusion occurring at this annealing temperature [20]. At the annealing temperature of 400 °C, the diffused indium was observed at the surface of glassy carbon. The loss of implanted indium due to evaporation occurred (Fig. 3) and the retained ratio decreased by about 2%

After annealing at 500 °C, the intensity of the indium depth profile reduced without further broadening compared to the 400 °C profile indicating migration and further loss of implanted indium as seen in

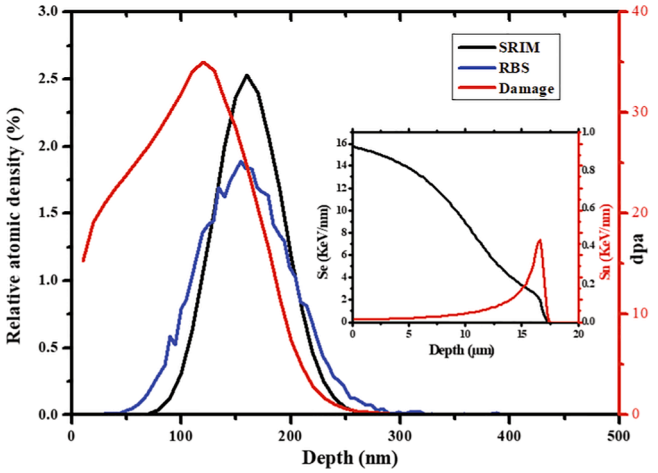

Fig. 1. Plots of the experimental Indium depth profile in glassy carbon after 360 keV In^+ implantation to the fluence of 1 × 10^{16} ions/cm^2, the SRIM-simulated In depth profile and the damage profile (dpa). Also included is the inset of simulated energy loss along target depth obtained using SRIM for the 167 MeV xenon irradiation.

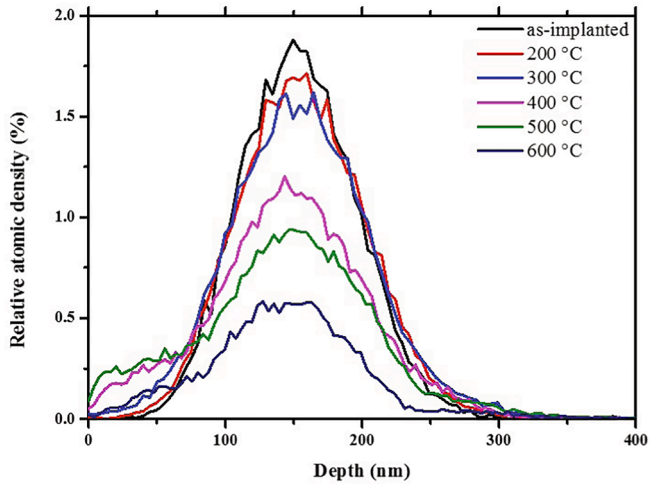

Fig. 2. Depth profiles of indium implanted in glassy carbon at room temperature compared with sample annealed sequentially from 200 to 600 °C for 1 h in steps of 100 °C.

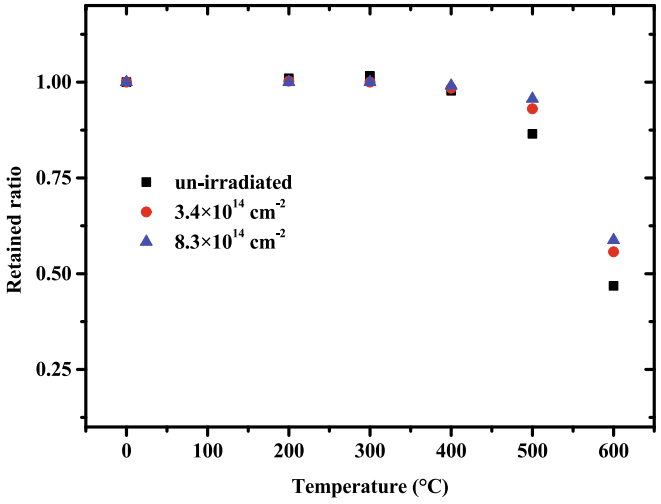

Fig. 3. Comparison of the indium retained within the glassy carbon substrate as a function of annealing temperature for the as-implanted sample and the sample implanted then SHI irradiated to fluences of 3.4 × 10^{14} and 8.3 × 10^{14} cm^{-2}.

Fig. 3. The projected range of the implanted indium did not shift compared to the as-implanted sample profile. This observation indicates that the implanted indium was trapped within the damaged region of glassy carbon. The retained ratio after annealing at 500 °C was found to be 86% as seen in Fig. 3. A slight deviation from the unimodal distribution of the indium profile was observed, which became asymmetric and no longer Gaussian, with some accumulation of indium near the surface of the glassy carbon. From Figs. 2 and 3, it is evident that there was a substantial loss of indium at a temperature of 600 °C. However, indium migration towards the pristine bulk was below the detection limits.

No significant migration of indium beyond the implantation-damaged region towards undamaged bulk was observed. This indicates the existence of a diffusion barrier that trapped the implanted indium within the damaged region. The diffusion of indium only occurred towards the surface where higher levels of implantation induced disorder was experienced. The migration of indium towards the surface is significant at 600 °C and the surface accumulation reduced. About 46% of indium was retained after annealing at 600 °C.

The structure of the pristine, implanted, implanted then SHI irradiated, implanted then annealed and the SHI irradiated then annealed samples were investigated by Raman spectroscopy analysis. The results from Raman spectroscopy analysis are shown in Fig. 4 (a) – (f). The first-order Raman spectrum of the pristine glassy carbon in Fig. 4 (a) shows the two characteristic peaks located at 1350 cm^{-1} (*D* peak) and 1585 cm^{-1} (*G* peak). The *D* peak indicates the presence of disorder - in the graphitic structure while the *G* peak is due to the in-plane vibrational mode of carbon sp^2 bonds. The Raman spectrum has another peak at 1620 cm^{-1} (D' peak) which is usually found in graphitic carbon materials with nano-sized sp^2 clusters [21–23].

The analysis of the pristine glassy carbon Raman spectrum was done by fitting the *D* and *G* peaks with Lorentzian and Breit-Wigner-Fano (BWF) functions respectively. The *D* and *G* peaks intensity ratio (I_D/I_G) of pristine glassy carbon was 1.4. Using the Tuinstra–Koenig equation [24], we calculated the average in-plane cluster size, L_a which found to be 3.1 nm. The Tuinstra–Koenig equation is valid for cluster sizes of between $2.5 < L_a < 300$ nm.

The Raman spectrum of implanted glassy carbon is shown in Fig. 4 (a) (black line). A broad peak can be observed after indium implantation and this is due to the merging of the *D* and *G* bands observed in the pristine sample. The *D* and *G* peak positions shifted to 1366 cm^{-1} and 1573 cm^{-1} respectively after indium implantation. The loss of the characteristic glassy carbon peaks and the peak shifts observed is usually

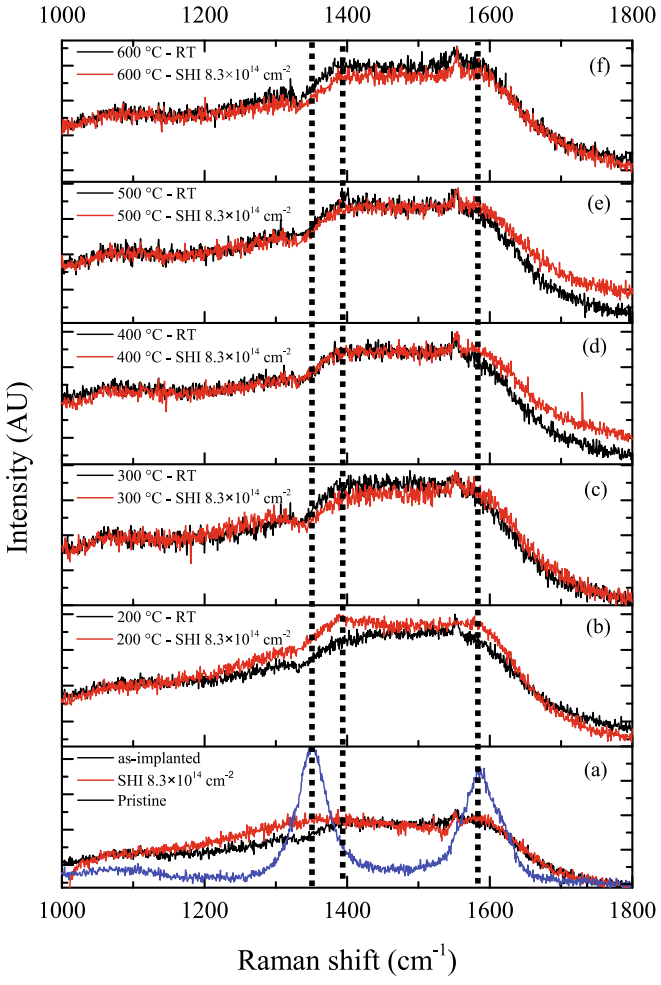

Fig. 4. Raman spectra of (a) pristine glassy carbon, after implantation with 360 keV indium ions compared to implanted glassy carbon then irradiated by 167 MeV Xe ions at room temperature to a fluence of 8.3 × 10^{14} cm^{-2}. (b) to (f) overlay of implanted and SHI irradiated samples after annealing from 200 °C to 600 °C.

interpreted as breaking up (damaging) of the nano-clusters within the indium implanted region. The Raman spectrum for the as-implanted sample was similar to that of amorphous carbon and this is due to the damaged structure of the implanted region of glassy carbon.

The 360 keV indium ions when penetrating the glassy carbon substrate lost energy by elastic collisions with the target atoms (nuclear stopping). During this process, atomic displacements from their lattice positions occurred near the glassy carbon surface. This displacement of atoms leads to distortion or damage in the glassy carbon structure. As stated previously, the 360 keV indium implantation has a maximum damage level of 34 dpa, therefore the glassy carbon substrate was expected to be damaged. It was previously reported that at damage levels greater than 4 dpa, the glassy carbon structure transforms to one close to that of amorphous carbon [13]. The implantation was also performed at room temperature, therefore structural recovery was suppressed and the implantation-induced disorder accumulated until the implantation fluence was attained. The accumulation of disorder in glassy carbon involves the breakdown of the graphitic ribbons observed in the pristine substrate, C interstitial atoms and vacancies.

The peak intensities ratio I_D/I_G reduced from 1.4 for the pristine glassy carbon to 0.97 after indium implantation. This is due to the damage induced by implantation and the reduction in the average cluster size. The small cluster size, L_a was calculated using the equation given by Ferrari et al. [21] since the Tuinstra–Koenig equation is no longer valid. A value of 1.3 nm was obtained and this confirmed that the implantation process resulted in a disordered layer with smaller cluster sizes. This damaged region has a higher density (2.04 g/cm^3) than that of pristine glassy carbon (1.42 g/cm^3).

The graphitic ribbons that exist in glassy carbon were broken by the indium implantation which resulted in a highly disordered layer and reduced the short-range order that exists in this material [5]. The downshift of the G band to the lower wavenumber and the decrease in the I_D/I_G ratio after In implantation suggest the relative decrease in sp^2 bonds fraction and the increase of sp^3 content in the modified layer [3,21]. Using the I_D/I_G ratios and applying the "amorphization trajectory" we can approximate that indium implanted glassy carbon consisted of between 10 and 15% sp^3 bonds compared to the pristine glassy carbon which primarily consists of sp^2 bonds.

The Raman spectra obtained after sequentially annealing the indium implanted glassy carbon substrate from 200 to 600 °C are shown in Fig. 4 (b) - (f). After annealing at 200 and 300 °C, there was a slight increase in *D* peak intensity. The general trend observed after annealing from 200 to 600 °C was the shift in the *D* peak position to lower wavenumbers accompanied by shift *G* peak to higher wavenumbers. After annealing a temperature of 600 °C, the *D* and *G* peaks became distinguishable near the positions of the pristine glassy carbon, especially the *G* peak.

Two opposing mechanisms govern the rate of defect annealing of the implanted samples. The first mechanism is temperature-induced recovery through the migration of carbon interstitials and vacancies within the glassy carbon substrate. The other is the migration of implanted indium within the damaged region. Slight recovery of the glassy carbon structure was observed after annealing up to temperatures of 600 °C. This is due to the two competing processes, that is, recovery and diffusion. Thermal annealing of the implantation damaged region at 600 °C leads to a slightly recovered layer. The proper recovery process is expected after all the implanted indium has diffused out as previously observed for the isothermally annealed samples [7]. Significant recovery of the implantation damage in glassy carbon was reported by Odutemowo et al. [25] to occur after annealing strontium implanted glassy carbon at 2000 °C.

3.2. Thermal annealing of the indium implanted and then SHI irradiated glassy carbon

In nuclear reactors, the fission process involves the release of nuclides with energies in the order of 100 MeV (SHIs energy regime). Since glassy carbon is envisaged for use as encapsulation material of high-level nuclear waste (HLW) and in nuclear reactors and it would be subjected to radiation.

SHI irradiation of glassy carbon can lead to structural changes along the ion trajectory. The charged energetic particles usually interact with both electrons and atomic nuclei in materials. The electronic energy loss along the trajectory of the 167 MeV Xe ions in glassy carbon was estimated using SRIM and the energy loss profiles are included Fig. 1. The maximum electronic energy loss was found to be about 15.7 keV nm^{-1} within the damaged region of the glassy carbon. Electronic energy loss which dominates near the surface rapidly declines towards the end of the ion track while the nuclear energy loss is very low close to the surface. This indicates that the main energy loss mechanism was by electronic excitations from inelastic collisions and not nuclear elastic collisions.

The depth profiles of indium implanted into glassy carbon and then irradiated with SHIs to fluences of 3.4 × 10^{14} and 8.3 × 10^{14} ions/cm^2 are shown in Fig. 5 (a) and (b), respectively. No detectable broadening, redistribution nor shift of the indium profiles was observed after irradiation with SHIs. This implies that the SHI irradiation did not induce migration of the implanted indium and that no sputtering (evaporation)

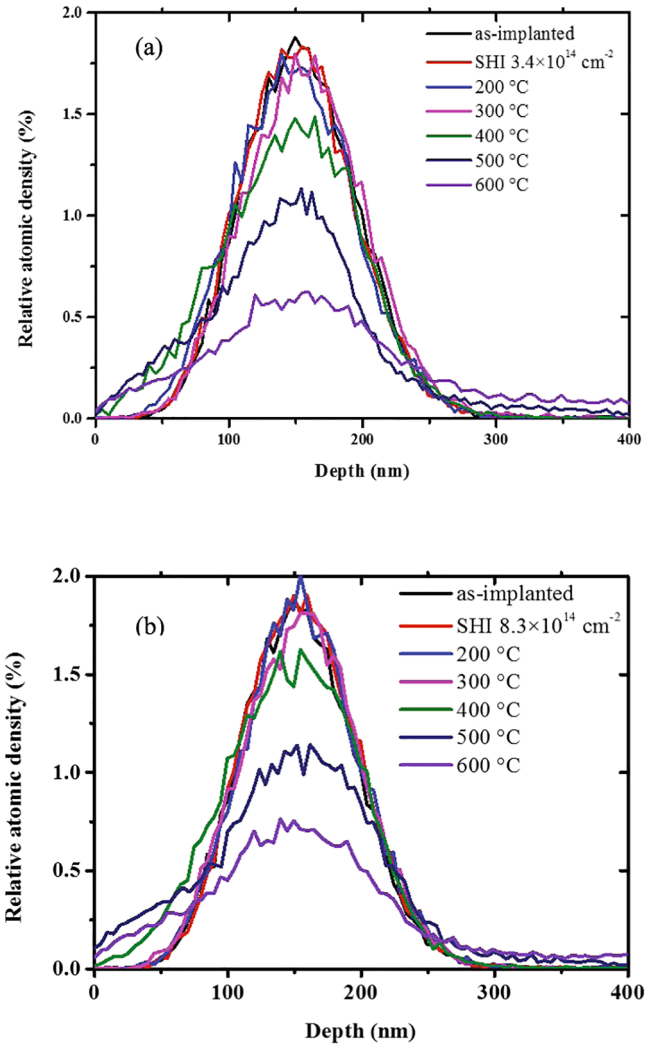

Fig. 5. Depth profiles of indium implanted glassy carbon then irradiated with 167 MeV Xe ions to a fluence of (a) 3.4 × 10^{14} cm^{-2} and (b) 8.3 × 10^{14} cm^{-2}. The SHI irradiated samples were annealed sequentially from 200 to 600 °C for 1 h.

of carbon from the damaged region was detected.

The two samples that had been irradiated with SHIs were sequentially annealed in vacuum from 200 to 600 °C. Annealing at 300 °C led to slight broadening, reduction in intensity and a slight shift of the indium profile towards the surface. This migration is still within the damaged region and no loss of implanted indium was observed, as seen from Fig. 3 where the retained ratios of the SHI irradiated samples annealed at 200 and 300 °C are almost 100%.

After annealing the samples irradiated with SHI to fluences of 3.4×10^{14} and 8.3×10^{14} ions/cm^2 at 400 °C, both the depth profiles broadened indicating an increase in the FWHM and decrease in intensity. The depth profiles shifted slightly towards the surface of the glassy carbon substrate, but there was no visible shift towards the bulk. The diffusion of implanted indium in the SHI irradiated sample that occurred at this temperature is to a lower degree compared to the implanted sample annealed at the same temperature, where the implanted indium had already diffused to the glassy carbon surface. The intensity of the indium profiles is also slightly higher than that of the annealed as-implanted sample. The shapes of the indium depth profiles of the SHI irradiated samples annealed at 400 °C, shown in Fig. 5, are also different from the just implanted samples. The SHI irradiated indium profiles still have a unimodal peak that is almost Gaussian and symmetric compared to the just implanted sample in Fig. 1 which has some form of surface accumulation and an asymmetric profile. The retained ratios of the SHI irradiated samples annealed at 400 °C, given in Fig. 3, are almost the same at about 100% compared to about 97% for the annealed as-implanted samples.

The indium depth profiles of SHI irradiated samples after annealing at 500 and 600 °C showed a further decrease in the indium peak intensity. After annealing at 500 °C, the intensity of the sample irradiated to a fluence of 3.4×10^{14} ions/cm^2 was lower than that irradiated to a fluence of 8.3×10^{14} ions/cm^2. A similar trend was also observed after annealing at 600 °C. The sample not irradiated with SHIs experienced a higher loss of implanted indium compared to the samples irradiated with SHI then annealed at 500 and 600 °C, as seen in Fig. 3.

The retained ratios of indium in samples irradiated with SHIs to fluences of 3.4×10^{14} and 8.3×10^{14} ions/cm^2 after annealing at 500 °C are 93% and 95% respectively compared to 86% for the annealed In implanted sample. At 600 °C, the retained ratio values of the SHI irradiated samples reduced to 55% and 58%, while that of the implanted and annealed sample was 46%. These observations indicate that there more loss of implanted indium in the annealed as-implanted sample than the implanted then SHI irradiated samples. The retained ratios of the SHI irradiated samples are almost the same since the fluence is within the same magnitude and might also be due to saturation of the ion track density.

Some of the damage introduced into the glassy carbon structure after RT indium implantation were annealed out during the SHI irradiation leading to different microstructures before commencing to anneal. Therefore, the diffusion behaviour of indium in the SHI irradiated samples was different from the one not irradiated with SHIs. There was enhanced retainment of implanted indium within the recovered structures (as seen in Fig. 3) and lower rates of diffusion were observed after annealing the SHI irradiated samples at 500 and 600 °C. These results indicate that SHI irradiation somehow retarded the diffusion of indium implanted into glassy carbon. The slight recovery in the SHI irradiated samples structure led to some form of trapping of implanted indium.

The diffusion coefficients for indium in glassy carbon were estimated by fitting the RBS depth profiles to the solution of Fick's equation for a Gaussian profile with a perfect sink at the surface [20]. The diffusion coefficients were extracted after sequential annealing (200–600 °C) from the broadening of implantation profiles of the In-implanted and the implanted then SHI irradiated samples in Figs. 2 and 5. A comparison of the calculated diffusion coefficients is given in Fig. 6.

The diffusion coefficients after the initial heating cycle at 200 °C are low and for the sample irradiated to a fluence of 8.3×10^{14} cm^{-2} is

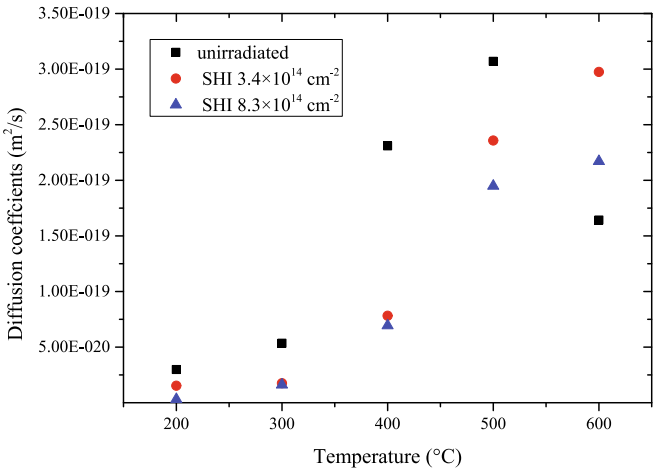

Fig. 6. Diffusion coefficients for the implanted and SHI irradiated samples annealed from 200 to 600 °C for 1 h.

almost at our detection limit of approximately 10^{-21} m^2 s^{-1}. This is due to the smaller peak broadening observed in Fig. 5 (b). The In implanted sample shows high diffusion coefficients over the annealing temperature range compared to the implanted and then SHI irradiated samples. At higher temperatures, that is 400 and 500 °C, the diffusion coefficients of the implanted sample were significantly higher than for the SHI irradiated samples. Although, at 600 °C, the out-diffusion of indium in the implanted but not irradiated with SHIs sample resulted in an inconsistent value which was lower than that for the SHI irradiated samples.

The conclusions one can draw is that indium diffusion is enhanced in the implanted and damaged glassy carbon and that localised defect annealing and defect restructuring due to SHI irradiation slowed down the diffusion processes of the implanted indium. This shows that some form of a trapping mechanism after SHI irradiation existed. No data for In diffusion in glassy carbon after SHI irradiation has been reported in literature. Therefore, we could not compare our diffusion coefficients with any literature values.

The effect of 167 MeV Xe^+ ions to fluences of up to 3.4×10^{14} and 8.3×10^{14} ions/cm^2 on the structure of indium implanted glassy carbon was investigated using Raman spectroscopy. The Raman spectra of RT 360 keV indium implanted glassy carbon then irradiated with SHIs to a fluence of 8.3×10^{14} ions/cm^2 and thereafter annealed in vacuum between 200 and 600 °C are shown in Fig. 4 (red line). The Raman spectrum of the implanted glassy carbon which was irradiated to a fluence of 3.4×10^{14} ions/cm^2 is not shown here since it is similar to that irradiated to a fluence of 8.3×10^{14} ions/cm^2 since the irradiation fluences are within the same magnitude.

The Raman spectrum of the sample irradiated with SHIs to a fluence of 8.3×10^{14} Xe ions/cm^2 still has the broad band but with a more visible *D* band which was not observed in the sample not irradiated with SHI, as seen in Fig. 4 (b). The *D* peak position after SHI irradiation shifted to lower wavenumber compared to as-implanted while the *G* peak position did not change. This indicates that the SHI irradiation caused some recovery within the implantation damaged region of glassy carbon. This reduced the implantation damage but to a low degree.

The incident 167 MeV Xe SHIs lose energy by inelastic collisions that produce electronic excitations. The electronic energy loss via electron–phonon coupling induces a very high local temperature which leads to a transient melt along the ion trajectories known as a thermal spike which is a high-temperature region formed along the trajectory of an energetic ion [26]. This transient melt process anneals out some of the pre-existing defects along the SHI trajectory leading to recovery by producing larger nano-clusters within the damaged region on glassy carbon. The recovery observed in Raman results was from the formation of small clusters during SHI irradiation from small seed structures within

the damaged layer. The microstructure of the near-surface region of the glassy carbon after SHI irradiation is different compared to as-implanted one. The annealing out of pre-existing implantation damage after SHI irradiation has been reported to occur by Williams et al. (Si, GaAs, InP, Ge-Si) [27], Wesch et al. (GaAs and InP), [28] and Zhang et al. (SiC) [29]. Complete recovery is not expected due to the short duration of the cooling process.

Annealing the SHI irradiated samples at 200 °C enhanced further recovery of the damaged region compared to the In implanted sample. The *D* and *G* peak intensities can be seen to be higher than the as-implanted sample. In amorphized carbon materials, the development of a *D* peak has been reported by Ferrari et al. to indicate ordering through an increase in the number of clusters [21].

However, after annealing at 300 °C, the initial recovery due to SHI irradiation is lost as the implanted indium started to rearrange and slightly migrate, as seen in Fig. 4 and Fig. 5 (b). At 400 °C and 500 °C, the *D* peak position and intensity was the same as the In implanted sample, but the *G* peak shifted to higher wavenumbers. While after annealing at 600 °C, the two spectra were almost similar. The as-implanted and the implanted then SHI irradiated samples had different structures before annealing and therefore resulted in different indium diffusion patterns as seen in the previous section. These results also indicate that indium diffusion influenced the restructuring of the SHI irradiated samples and the recovered regions were damaged by the diffusion of Indium. The lowered rate of diffusion or higher retention of indium after SHI irradiation could be ascribed to restructuring and enhanced trapping induced by the electronic energy loss.

4. Conclusions

The structural effects and migration of indium implantation into Sigradur® G glassy carbon, after swift heavy ion irradiation with 167 MeV Xe before and after annealing were studied. The implantation of glassy carbon with 360 keV indium ions was observed to damage the glassy carbon structure. Raman measurements indicated that under the implantation conditions, the glassy carbon structure was damaged. The glassy carbon substrates implanted with indium were irradiated with 167 MeV SHI Xe ions up to fluences of 3.4 and 8.3 $\times$ 10^{14} cm^{-2}. The results suggested that swift heavy ion irradiation did not enhance the migration of implanted indium in glassy carbon but rather reduced it. The results demonstrate that swift heavy ion irradiation with electronic energy deposition of about 11 keV nm^{-1} induced modification of structural properties of the pre-implanted glassy carbon (damage annealing).

Raman analysis demonstrated that the annealing out of implantation damage led to slight recovery after RT SHI irradiation. The transient thermal spikes induced by SHIs along their path within the damaged region of glassy carbon produced intense heating, which is the origin of the recovery phenomenon observed upon SHI irradiation of damaged glassy carbon. The implanted and SHI irradiated specimen which exhibited different defect structures, that is damaged and partially recovered, respectively, were annealed from 200 to 600 °C. The migration behaviour of implanted indium in glassy carbon was different, and more indium was retained at each temperature for SHI irradiated samples compared to non-irradiated samples. This is due to the different structures observed from Raman analysis of the implanted and SHI irradiated samples. The electronic energy loss induced recovery process and the higher retention of implanted indium and this has some implications for material performance evaluation in extreme radiation environments.

CRediT authorship contribution statement

E.G. Njoroge: Conceptualization, Methodology, Investigation, Writing - original draft. **T.T. Hlatshwayo:** Investigation, Writing - review & editing. **M. Mlambo:** Investigation, Writing - review & editing. **O. Odutemowo:** Writing - review & editing. **K.A. Annan:** Investigation, Writing - review & editing. **V.A. Skuratov:** Investigation, Resources, Writing - review & editing. **M. Ismail:** Investigation, Writing - review & editing. **J.B. Malherbe:** Resources, Writing - review & editing, Supervision.

Declaration of Competing Interest

The authors declare that they have no known competing financial interests or personal relationships that could have appeared to influence the work reported in this paper.

Acknowledgements

Financial support from the National Research Foundation (NRF) of South Africa (120082, 115865) and the University of Pretoria (A1A706) is gratefully acknowledged. The authors appreciate Prof. Elke Wendler, and the technical staff at the Institut für Festkörperphysik, Friedrich-Schiller-Universität Jena, Germany, for their assistance with the ion implantation.

References

[1] A.F. Craievich, On the structure of glassy carbon, Mater. Res. Bull. I 11 (10) (1976) 1249–1255.
[2] G.M. Jenkins, K. Kawamura, Polymeric Carbons – Carbon Fibre, Glass and Char, Cambridge University Press, Cambridge, 1976.
[3] V. Lavrentiev, J. Vacik, H. Naramoto, Structural phenomena in glassy carbon induced by cobalt ion implantation, Appl. Phys. A Mater. Sci. Process. 92 (3) (2008) 673–680.
[4] P.J.F. Harris †, Fullerene-related structure of commercial glassy carbons, Philos. Mag. 84 (29) (2004) 3159–3167.
[5] H. Saitoh, T. Shinada, Y. Ohkawara, S. Ohshio, H. Hiraga, T. Inoue, Surface modification of glassy carbon by pulsed laser irradiation with several wavelengths, J. Appl. Phys. 41 (Part 1, No. 8) (2002) 5359–5366.
[6] P.K. Chu, L. Li, Characterization of amorphous and nanocrystalline carbon films, Mater. Chem. Phys. 96 (2-3) (2006) 253–277.
[7] E.G. Njoroge, L.D. Sebitla, C.C. Theron, M. Mlambo, T.T. Hlatshwayo, O. S. Odutemowo, V.A. Skuratov, E. Wendler, J.B. Malherbe, Structural modification of indium implanted glassy carbon by thermal annealing and SHI irradiation, Vacuum. 144 (2017) 63–71.
[8] N.L. Pocard, D.C. Alsmeyer, R.L. McCreery, T.X. Neenan, M.R. Callstrom, Doped glassy carbon: a new material for electrocatalysis, J. Mater. Chem. 2 (1992) 771–784.
[9] O.J.A. Schueller, S.T. Brittain, C. Marzolin, G.M. Whitesides, Fabrication and characterization of glassy carbon MEMS, Chem. Mater. 9 (6) (1997) 1399–1406.
[10] Y.S. Virgil'ev, I.G. Lebedev, Effect of neutron irradiation on properties of glassy carbon, Inorg. Mater. 38 (2002) 668–673.
[11] O.S. Odutemowo, J.B. Malherbe, C.C. Theron, E.G. Njoroge, E. Wendler, In-situ RBS studies of strontium implanted glassy carbon, Vacuum 126 (2016) 101–105.
[12] V. Bernardet, S. Gomes, S. Delpeux, M. Dubois, K. Guérin, D. Avignant, G. Renaudin, L. Duclaux, Protection of nuclear graphite toward fluoride molten salt by glassy carbon deposit, J. Nucl. Mater. 384 (3) (2009) 292–302.
[13] D.G. McCulloch, S. Prawer, A. Hoffman, Structural investigation of xenon-ion-beam-irradiated glassy carbon, Phys. Rev. B 50 (9) (1994) 5905–5917.
[14] M. Iwaki, K. Terashima, Change in atomic density of glassy carbon by Na ion implantation, Surf. Coatings Technol. 128-129 (2000) 429–433.
[15] D. McCulloch, A. Hoffman, P.J. Evans, S. Prawer, Structural and chemical bonding investigation of tungsten implanted glassy carbon, Nucl. Inst. Methods Phys. Res. B. 80-81 (1993) 1460–1463.
[16] S.A. Adeojo, J.B. Malherbe, E.G. Njoroge, M. Mlambo, O.S. Odutemowo, T. Thabethe, Z.A.Y. Abdalla, T.T. Hlatshwayo, Effect of sequential isochronal annealing on the structure and migration behaviour of selenium-ion implanted in glassy carbon, Vacuum. 182 (2020), 109689.
[17] D. McCulloch, A. Hoffman, S. Prawer, Ion-beam induced compaction in glassy carbon, J. Appl. Phys. 74 (1) (1993) 135–138.
[18] J.F. Ziegler, SRIM-2013, Www.SRIM.Org. (2013). http://www.srim.org.
[19] A. Hoffman, H. Geller, I. Gouzman, C. Cytermann, R. Brener, M. Kenny, Formation of carbon nitride films by high-energy nitrogen ion implantation into glassy carbon, Surf. Coatings Technol. 68-69 (1994) 616–620.
[20] J.B. Malherbe, P.A. Selyshchev, O.S. Odutemowo, C.C. Theron, E.G. Njoroge, D. F. Langa, T.T. Hlatshwayo, Diffusion of a mono-energetic implanted species with a Gaussian profile, Nucl. Inst. Methods Phys. Res. B. 406 (2017) 708–713.
[21] A.C. Ferrari, J. Robertson, Interpretation of Raman spectra of disordered and amorphous carbon, Phys. Rev. B. 61 (20) (2000) 14095–14107.
[22] T. Kozu, M. Yamaguchi, M. Kawaguchi, H. Shima, J.W. Kim, M. Matsuoka, K. Nishida, T. Yamamoto, Evaluating of Diamond Like Carbon Using Deep UV Raman Spectroscopy, Integr. Ferroelectr. 157 (1) (2014) 147–156.

[23] T.R. Ravindran, B.R. Jackson, J.V. Badding, UV Raman spectroscopy of single-walled carbon nanotubes, Chem. Mater. 13 (11) (2001) 4187–4191.
[24] F. Tuinstra, J.L. Koenig, Raman spectrum of graphite, J. Chem. Phys. 53 (3) (1970) 1126–1130.
[25] O.S. Odutemowo, J.B. Malherbe, L. Prinsloo, D.F. Langa, E. Wendler, High temperature annealing studies of strontium ion implanted glassy carbon, Nucl. Instruments Methods Phys. Res. B. 371 (2016) 332–335.
[26] M. Toulemonde, C. Dufour, E. Paumier, Transient thermal process after a high-energy heavy-ion irradiation of amorphous metals and semiconductors, Phys. Rev. B. 46 (22) (1992) 14362–14369.
[27] J.S. Williams, M.C. Ridgway, R.G. Elliman, J.A. Davies, S.T. Johnson, G.R. Palmer, MeV ion-beam annealing of semiconductor structures, Nucl. Instruments Methods Phys. Res. B. 55 (1-4) (1991) 602–606.
[28] W. Wesch, A. Kamarou, E. Wendler, K. Gärtner, P.I. Gaiduk, S. Klaumünzer, Ionisation stimulated defect annealing in GaAs and InP, Nucl. Instruments Methods Phys. Res. B. 206 (2003) 1018–1023.
[29] Y. Zhang, R. Sachan, O.H. Pakarinen, M.F. Chisholm, P. Liu, H. Xue, W.J. Weber, Ionization-induced annealing of pre-existing defects in silicon carbide, Nat. Commun. 6 (2015) 1–7.